






Review

Properties of Barium Cerate-Zirconate Thin Films

Piotr Winiarz ¹, Monica Susana Campos Covarrubias ², Mantas Sriubas ², Kristina Bockute ²,
Tadeusz Miruszewski ¹, Wojciech Skubida ¹, Daniel Jaworski ¹, Giedrius Laukaitis ² and Maria Gazda ^{1,*}

- ¹ Institute of Nanotechnology and Materials Engineering, Faculty of Applied Physics and Mathematics and Advanced Materials Centre, Gdańsk University of Technology, Narutowicza 11/12, 80-233 Gdańsk, Poland; piotr.winiarz1@pg.edu.pl (P.W.); tadeusz.miruszewski1@pg.edu.pl (T.M.); wojciech.skubida@pg.edu.pl (W.S.); daniel.jaworski@pg.edu.pl (D.J.)
- ² Physics Department, Kaunas University of Technology, Studentu Str. 50, LT-51368 Kaunas, Lithuania; monica.campos@ktu.lt (M.S.C.C.); mantas.sriubas@ktu.lt (M.S.); kristina.bockute@ktu.lt (K.B.); giedrius.laukaitis@ktu.lt (G.L.)
- * Correspondence: maria.gazda@pg.edu.pl

Abstract: In this work, we review several experimental results showing the electrical properties of barium cerate-zirconate thin films and discuss them in view of the possible influence of various factors on their properties. Most of the presented Ba(Ce, Zr, Y)O₃ thin films were formed by the pulsed laser deposition (PLD) technique, however thin films prepared using other methods, like RF magnetron sputtering, electron-beam deposition, powder aerosol deposition (PAD), atomic layer deposition (ALD) and spray deposition are also reported. The electrical properties of the thin films strongly depend on the film microstructure. The influence of the interface layers, space-charge layers, and strain-modified layers on the total conductivity is also essential but in many cases is weaker.

Keywords: BaZrO₃; thin films; microstructure; interfaces; strain; electrical properties



Citation: Winiarz, P.; Covarrubias, M.S.C.; Sriubas, M.; Bockute, K.; Miruszewski, T.; Skubida, W.; Jaworski, D.; Laukaitis, G.; Gazda, M. Properties of Barium Cerate-Zirconate Thin Films. *Crystals* **2021**, *11*, 1005. <https://doi.org/10.3390/cryst11081005>

Academic Editor: Anna Paola Caricato

Received: 13 August 2021

Accepted: 19 August 2021

Published: 23 August 2021

Publisher's Note: MDPI stays neutral with regard to jurisdictional claims in published maps and institutional affiliations.



Copyright: © 2021 by the authors. Licensee MDPI, Basel, Switzerland. This article is an open access article distributed under the terms and conditions of the Creative Commons Attribution (CC BY) license (<https://creativecommons.org/licenses/by/4.0/>).

1. Introduction

The first inorganic thin films were produced in Egypt around 3000BC [1]. Egyptians produced gold films for decorative applications with a thickness of roughly a few microns. The advancement of vacuum technology in the nineteenth century led to new sputtering techniques such as physical vapour deposition (PVD) [2], where the parameters during the deposition have greater controllability than previous methods. Lastly, in the middle of the 20th century, the development of field-effect transistors and thin-film transistors forced scientists to the evolution of chemical vapour deposition methods. A lot of different techniques are commonly known, such as sputtering techniques, Langmuir-Blodgett film deposition, sol-gel method, spin coating, dip coating and many others. Interestingly, there is not a precise definition of thin films, because different properties scale differently with the thickness. However, we can say that the limit below we can use the adjective “thin” is the thickness under which the considered anomaly of a physical phenomenon occurs [3]. Thin films are commonly manufactured and used in many areas, including transparent electronics [4], piezoelectric- [5] and thermoelectric devices [6], solar cells [7] and multiferroic heterostructures [8]. To obtain the desired properties of a certain material or a device, one has to select an adequate technique and control the physical process of the thin film deposition. What should be remembered while a device composed of at least one thin layer deposited on a substrate is considered is that the film may be strained as a result of structural differences between the substrate and the thin film. It is important since many film properties have been found to depend on strain. In general, when an external force pulls an object and causes an elongation, we call it tensile stress, and when it is compressed,

we have compressive stress. The quantity which describes this deformation is called strain. The relation between stress σ and strain ε is expressed in Equation (1):

$$\sigma = Y\varepsilon \quad (1)$$

where Y is an elastic modulus, which is called either Young modulus or bulk modulus or shear modulus, depending on if the stress is tensile, bulk, or shear respectively. This modulus does not have to be linear, hence properties of the strained material may be complex. In materials science, the strain may be induced in a thin film material by means of: choice of a substrate, choice of type and parameters of the deposition process, mismatch of thermal expansion coefficients (TECs) between the film and substrate, and by chemical methods by using specifically chosen dopants. The structural origins of strain, in particular, the unit cell parameters mismatch as well as TEC difference between the film and substrate are illustrated in Figure 1.

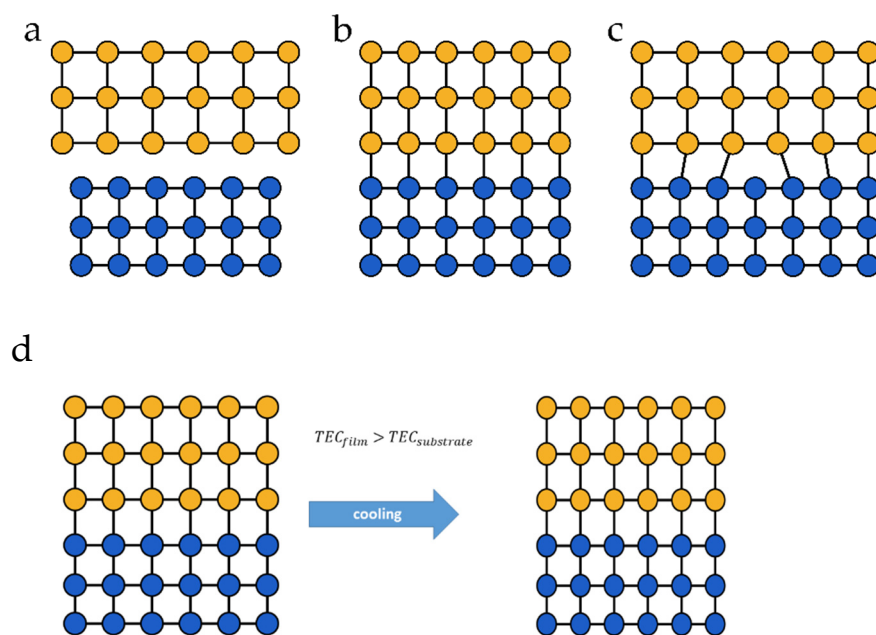


Figure 1. Origins of the strain in a thin film: (a) illustration of a lattice mismatch of the film (yellow) and the substrate (blue); (b) elastically strained film; (c) a misfit dislocation which forms if a lattice mismatch exceeds a critical value; (d) if the film and the substrate differ in TEC, at the temperature of a deposition only the strain originating from the lattice mismatch is present but below or above the deposition temperature, an additional contribution to strain appears. If $TEC_{film} > TEC_{substrate}$ at temperatures below the deposition temperature, the film is additionally compressed.

The impact of strain on the transport properties and band structure of semiconductors was first investigated theoretically by Bardeen and Shockley in 1950 [9] and measured experimentally in 1954 by Smith [10]. After over 30 years of research on piezoresistance, strain altered bulk charge carrier mobility, and deformation potential, the first strain-engineered MOSFET was reported by Welser et al. in 1992 [11]. Since that time, strain engineering has become a powerful tool and is widely applied on an industrial scale in modern semiconductor devices [12,13]. What is important, the applications of strain engineering are not limited only to semiconductors. The strain has been also used to alter thermal, magnetic, optical and phonon properties in many different material systems [14–16]. Recently, strain engineering has also been employed in electroceramic thin films. While the general relationships between electrical, mechanical and chemical properties of electroceramics were recognized decades ago, the realization that this three-way electro-chemo-mechanical coupling can be used simultaneously as a tool to engineer materials with vastly improved characteristics is a very recent one. The term itself was introduced by Tuller et al. in

2011 [17]. So far, the influence of strain on ionic conductivity has been explored mainly for oxygen ion conductors such as yttrium-stabilized zirconia, cerium oxide or doped perovskites [18–21]. Proton ceramic conductors have not received much attention yet in this field.

Proton ceramic conductors are inorganic oxides in which proton defects, namely hydroxide ions occupying lattice oxygen sites (OH_O^\bullet), are mobile. The state-of-art proton-conducting oxides are perovskites based on barium cerate and zirconate ($BaCeO_3$ and $BaZrO_3$). Proton defects in these oxides form via the hydration reaction (Equation (2)) in an atmosphere containing water vapour [22]. The hydration reaction involves oxygen vacancies ($v_O^{\bullet\bullet}$), therefore, for achieving a significant proton defect concentration, the presence of oxygen vacancies is necessary. Due to a relatively small concentration of intrinsic defects in oxides, extrinsic oxygen vacancies are introduced through acceptor-type doping.



In the case of barium zirconate/cerate, an often used acceptor is yttrium (Y^{3+}) substituted for zirconium or cerium (Zr^{4+} , Ce^{4+}). Consequently, the charge neutrality condition requires that the oxygen content per formula is lower than 3, that is, the actual formulae of acceptor-doped compounds are: $BaCe_{1-x}Y_xO_{3-\delta}$ and $BaZr_{1-x}Y_xO_{3-\delta}$, where δ depends on x , atmosphere and temperature. Proton transport is a thermally activated two-step process [23]. The first step, so-called rotational diffusion involves the rotation of the O-H bond, whereas the second one is a proton hop from its initial oxygen to a neighbouring one. The activation energy of conduction originates mainly from the second step.

It should be stressed that proton-conducting oxides are very prospective and interesting materials since they may be practically applied as electrolytes in such electrochemical devices as proton ceramic fuel cells (PCFC), electrolyzers, gas sensors, etc. These devices are usually multi-layer systems in which particular materials are in contact one with another and, as a result, may be strained.

In this work, we review several experimental results showing the electrical properties of barium cerate-zirconate films and discuss them in view of the possible influence of strain and other factors on their properties.

1.1. Barium Cerate-Zirconate Films with Intentionally Introduced Strain

So far, there have been only three experimental works devoted to studies of strained barium cerate-zirconate films in which strain was introduced intentionally.

The first attempt of studying the strained proton-conducting barium zirconate was reported by Yang et al. [24]. They studied strongly strained $BaZr_{0.8}Y_{0.2}O_{3-\delta}$ (BZY) interfaces formed with the PLD method as very thin films (5–500 nm) deposited on the (110) $NdGaO_3$ (NGO) perovskite single crystalline substrates. They found that the BZY-substrate interfacial layer of about 20 nm thickness is strained because of the lattice mismatch between NGO and the film. This strain strongly influences the defect concentration, which in turn affects the conductivity of the film. The authors discussed also the presence of a space charge layer related to the phenomena occurring in the junctions between the film and the metallic electrode. They postulated that the strain in the interface layer enables a higher concentration of charge carriers, i.e., proton defects, whereas, in the space charge layer the concentration of charge carriers is lower. The values and activation energy of conductivity of the films depended on their thickness, interestingly, very thin films (10–20 nm) showed higher conductivity and lower activation energy (0.50–0.55 eV) in comparison with 100–500 nm films (0.75–0.80 eV).

Fluri et al. reported very thorough studies on strained $BaZr_{0.8}Y_{0.2}O_{3-\delta}$ films deposited on the MgO single crystal substrate [25]. The films were deposited using the pulsed laser deposition (PLD) method in a vacuum, with a substrate temperature of 750 °C. The Y-doped barium zirconate films were epitaxial with columnar morphology. The strain in the films was related to the mismatch between the unit cell parameters of the substrate and the film and was controlled by using the $BaZr_{0.6}Ce_{0.4}O_3$ buffer layer. They found that ten-

sile in-plane strain, through lowering the proton-dopant association energy, increases the proton conductivity in the plane, whereas the compressive in-plane strain decreases the conductivity. That was also accompanied by a change in proton migration activation energy.

The third experimental attempt of studying the influence of strain on the proton conductivity was our previous work in which we investigated the structural and electrical properties of metal-supported thin films of barium cerate [26]. The electron-beam deposition process was carried out with the 12 Å/s rates and the substrate temperature of 600 °C. In this case, the strain in barium cerate films was induced by the difference of TECs between the barium cerate and the used substrate. The materials used as substrates were commercial metal alloys: Invar, Glass sealing alloy, Inconel, and Stainless steel. The substrate composition varied one from another but all contained mainly Fe, Ni, Cr and Co. The thermal expansion coefficient of the materials was respectively, 1.8, 4.8, 13 and 18×10^{-6} 1/K, whereas for the barium cerate it is around 11×10^{-6} 1/K [27]. Therefore, either compressive or tensile in-plane strain at temperatures below 600 °C was present in the films. The films were polycrystalline but had oriented, cubic perovskite structures regardless of their strain origin. Due to the presence of metallic substrates, only the conductivity perpendicular to the plane was measured. It was found that the film with the highest in-plane tensile strain showed the lowest activation energy of total conductivity, whereas the film with the lowest in-plane strain showed the highest values of total conductivity.

1.2. Barium Cerate-Zirconate Films without Intentionally Introduced Strain

Apart from the above three works devoted to the strain influence on the barium cerate-zirconate proton conductors, several reports concerning thin and thick films of barium cerate-zirconates were published. The most often used deposition method was the pulsed laser deposition (PLD) technique, however other methods, e.g., powder aerosol deposition (PAD), atomic layer deposition (ALD) and spray deposition were also reported. The substrates which were used for the deposition varied, for example, they were single crystalline (e.g., MgO, Al₂O₃) polycrystalline (e.g., Al₂O₃) and amorphous (SiO₂).

First, exemplary films obtained using the pulsed laser deposition method will be described. The work by D. Pergolesi et al. presented very interesting results concerning the electrical properties of yttrium-doped barium zirconate films (BaZr_{0.8}Y_{0.2}O_{3-δ}) deposited by PLD on the MgO and Al₂O₃ single-crystalline substrates [28]. The substrate temperature during the deposition process was 600 °C. They found that the proton conductivity of the BZY films deposited on the MgO and Al₂O₃ substrates was, respectively, two orders of magnitude and about 40 times higher than that of the bulk material. The activation energy of conductivity was equal to 0.63 eV in both cases. What is interesting, the authors did not observe the dehydration of the films up to 600 °C. Different properties of the thin films and the bulk sintered ceramics were explained based on the microstructural differences between them.

Shim et al. presented proton conductivity in BaZr_{0.8}Y_{0.2}O_{3-δ} films grown using the PLD method on the MgO (100) substrate heated to 780 °C [29]. They studied the films with different thicknesses ranging from 60 nm to 670 nm and observed the dependence of conductivity on the film thickness. The conductivity of the BaZr_{0.8}Y_{0.2}O₃ films on MgO was compared with that of the films deposited on amorphous quartz supports. The total conductivity of the films deposited on MgO was comparable to that of the bulk samples. Also, the activation energy of conductivity of the films on MgO (0.44–0.46 eV) was similar to the reference value (0.44 eV). On the other hand, the conductivity of the films deposited on quartz was much lower (2–4 orders of magnitude) while the activation energy was higher (1.2 eV) in comparison to the bulk ceramics. Further development of this research was performed by Kim et al. [30]. The deposition process was carried out using quartz substrates at the temperature between 400 °C and 900 °C and MgO (100) substrates at the temperature between 600 °C and 900 °C. The authors found that the conductivity of the films strongly depends on the type and temperature of the substrate utilized for the deposition. In agreement with the previous work, they confirmed that both the value

and activation energy of conductivity of the films deposited on MgO differed from those on the amorphous quartz. In the case of the MgO substrates, the activation energy of conductivity was 0.45 eV and 0.51–0.53 eV for the films deposited at 800–900 °C and 600–700 °C, respectively. The activation energy of conductivity of the films deposited on the quartz substrates was 1.12 eV. The authors interpreted the dependence of the properties of the film on the characteristics of the deposition process and on the film thickness as related to the changes in their crystallinity and microstructure.

Hosono et al. studied doped barium cerate films ($\text{BaCe}_{0.9}\text{Y}_{0.1}\text{O}_3$) deposited on MgO (100) by pulsed laser deposition [31]. They studied the film growth with the substrate temperature between 450 and 700 °C and found 600 °C as the temperature most suitable for the formation of preferably *c*-axis oriented film. The thickness of the films was 700 nm. The electrical properties of the films were typical of the proton conductors, that is, the conductivity in the wet atmosphere was higher than in the dry one and the isotope effect was observed, however, the activation energy of conductivity in the wet atmosphere was high (0.92 eV in the temperature range from 350 and 700 °C).

Magrasó et al. deposited $\text{BaZr}_{0.9}\text{Y}_{0.1}\text{O}_{3-\delta}$ with the PLD method [32]. They characterized the films deposited on single-crystalline oxides with different structure types, e.g., MgO, GdScO₃, SrTiO₃, NdGaO₃, LaAlO₃ and sapphire. The substrate temperature was between 600 and 800 °C. The lattice mismatch between the film and the substrate provides additional in-plane strain, ranging from +0.2% tensile strain for MgO substrate and –16.7% compressive strain for a sapphire. The electrical conductivity for 35 nm film on MgO exceeded $10^{-2} \text{ S}\cdot\text{cm}^{-1}$ at 700 °C in dry/wet argon and wet air. The authors observed the effect of hydration similar to the one observed in bulk proton-conducting materials. The activation energy of conductivity was 0.65 eV in wet and 0.80 eV in dry atmospheres.

Another example showing the electrical properties of the $\text{BaZr}_{0.85}\text{Y}_{0.15}\text{O}_{3-\delta}$ films deposited with the PLD method on MgO (100) was reported by Bae et al. [33]. The authors found that the conductivity of nanocrystalline films was two orders of magnitude lower than that of microcrystalline sintered BZY. The activation energy of conductivity was approximately 0.79 eV.

Surprisingly, only a few examples of reports showing the properties of films grown using other sputtering methods have been published so far. Yazdi et al. presented the properties of the films of various barium and strontium cerate-zirconates deposited using the reactive magnetron sputtering method [34,35]. In the first work [35], the authors performed an extensive comparison of the structural and electrical properties of bulk- and thin-film materials. They studied relatively thick (6 µm) $\text{BaZr}_{0.84}\text{Y}_{0.16}\text{O}_{3-\delta}$ films deposited on the alumina substrates covered with a 200 nm film of Pt₃Ti functioning as a current collector. The BZY film crystallized in situ with the substrate heated to 250 °C for two hours. Further crystallization proceeded during the first heating to 675 °C and annealing at this temperature for 12 h. Total conductivity in the dry atmosphere of the film was lower than that of the dense ceramic pellet. They determined the activation energy of the total conductivity of the films and the bulk sample below 400 °C as 0.62 eV and 0.52 eV, respectively, while between 400 and 700 °C as 0.36 eV and 0.76 eV, respectively. Yazdi et al. in their further work [34] compared properties of $\text{SrZr}_{0.84}\text{Y}_{0.16}\text{O}_{3-\delta}$ (SZY16), $\text{BaZr}_{0.84}\text{Y}_{0.16}\text{O}_{3-\delta}$ (BZY16), $\text{BaCe}_{0.8}\text{Zr}_{0.1}\text{Y}_{0.1}\text{O}_{3-\delta}$ (BCZY10), and $\text{BaCe}_{0.90}\text{Y}_{0.10}\text{O}_{3-\delta}$ (BCY10) thin films deposited by reactive magnetron sputtering. They found that the conductivity of the films is always lower in comparison to the bulk materials. Lin-Jung Wu and Jenn-Ming Wu [36] reported properties of sputtered platinum-doped lead barium zirconate ($\text{Pb}_{0.6}\text{Ba}_{0.4}$) ZrO₃ thin films deposited on Pt (150 nm)/Ti/SiO₂/Si substrates by RF magnetron sputtering. The authors discussed the influence of internal stress present in the films on the mechanisms of electronic transport. Lead barium zirconate does not belong to proton-conducting materials, however, because of the structural similarities between zirconate perovskites, similar phenomena may be present in these materials.

The atomic layer deposition method (ALD) as one of the chemical methods of thin film growing was applied in relation to the barium cerate-zirconate materials by J.S. Park

et al. [37]. They studied the ionic conductivity of atomic layer deposited films of yttrium-doped barium zirconate films. The 150 nm $\text{Ba}_y\text{Zr}_{0.8}\text{Y}_{0.2}\text{O}_{3-\delta}$ (with y between 0.4 and 1.6) films deposited on quartz substrates were further annealed at 700–900 °C in air. The authors studied the influence of barium content on the conductivity of the films. They found that the highest conductivity corresponded to the stoichiometric barium content ($y = 1$). On the other hand, the activation energy was between 0.80 eV and 0.87 eV regardless of the barium content. J. An et al. studied 50 nm films of $\text{BaZr}_{0.8}\text{Y}_{0.2}\text{O}_{3-\delta}$ deposited on Si(100) substrate using ALD [38]. They found that the presence of the perfluoroelastomer O-ring used for vacuum sealing may be a source of fluorine contamination of the films. Similar to the previous results, they found the activation energy of conductivity below 550 °C of the films not containing fluorine was equal to 0.77 eV.

Dense Y-doped perovskite films of $\text{BaZr}_{0.8}\text{Y}_{0.2}\text{O}_{3-\delta}$ (BZY20) and $\text{BaCe}_{0.8}\text{Y}_{0.2}\text{O}_{3-\delta}$ (BCY20) were studied by Exner et al. [39,40]. The films were deposited at room temperature by powder aerosol deposition (PAD) on polycrystalline alumina with platinum interdigital electrodes (IDE). The 2–10 μm thick films consisting of nonoriented strained nanograins (BZY20 and BCY20 showed the compressive strain of 0.25% and 0.2%, respectively) were dense even without sintering, however, they were heat-treated during the electrical analyses conducted in the temperature range between 300 and 1000 °C. The authors found that the thermal annealing performed in the heating step of electrical conductivity measurements enhanced the conductivity of the films. In particular, the conductivity at 400 °C of the BZY20 film increased by approximately 3 orders of magnitude, whereas the activation energy of conductivity changed from 1.73 eV to 0.88 eV. In the case of BCY20, annealing caused an increase in conductivity by a factor of 38, while the activation energy before and after annealing was 0.99 eV and 0.54 eV, respectively. The authors interpreted the influence of annealing on electrical properties as related to the release of the strain which may be at high temperatures. What is also interesting, the hardness of the films was significantly higher than that of the bulk samples.

Properties of the polycrystalline $\text{BaZr}_{0.9}\text{Y}_{0.1}\text{O}_{3-\delta}$ (BZY10) films deposited on the alumina substrates using the ink-jet printing method were reported by Schneller et al. [41]. The electrical conductivity of the films was lower than that of the bulk ceramic material. The activation energy of conductivity was 0.56 eV below 400 °C and 1.46 eV above this temperature.

One of the common, simple and economical methods for thin film deposition is the spray pyrolysis technique. Dubal et al. presented dense and nanocrystalline $\text{BaCe}_{0.7}\text{Zr}_{0.1}\text{Y}_{0.2}\text{O}_{2.9}$ (BCZY712) thin films obtained by spraying the previously prepared nitrates on the alumina substrate at 250 °C [42]. Further annealing at 1000 °C led to the formation of single-phase, dense, polycrystalline BCZY712 films. The authors showed that the total conductivity of the film in dry and humidified air at 400 °C is, respectively, $0.71 \times 10^{-3} \text{ S}\cdot\text{cm}^{-1}$ and $0.83 \times 10^{-3} \text{ S}\cdot\text{cm}^{-1}$. The noticed difference suggests the proton contribution in the humid atmosphere. The activation energy of total conductivity in the humid air was 0.73 eV.

Finally, what should be also mentioned in this review of the properties of thin films of barium cerate-zirconate thin films, are the attempts of construction of thin-film proton-conducting fuel cells (PCFC). For instance, Yoo and Lim presented an efficient anode-supported PCFC with the 10–15 μm thick electrolyte of $\text{Ba}_{0.98}\text{Ce}_{0.6}\text{Zr}_{0.2}\text{Y}_{0.2}\text{O}_{3-\delta}$ [43]. The highest power density in wet powder sprayed and co-fired cell ($493 \text{ mW}\cdot\text{cm}^{-2}$) was achieved at 600 °C and 0.7 V in the atmosphere of humid 75% H_2 in Ar. The higher power density was reported by K. Bae et al. [33] in a PCFC in which the 2.5 μm $\text{BaZr}_{0.85}\text{Y}_{0.15}\text{O}_{3-\delta}$ electrolyte was deposited on the anode using the PLD method. The authors reported that the optimized PCFC showed a high power density of $740 \text{ mW}\cdot\text{cm}^{-2}$ at 600 °C and high OCV of about 1 V. They attributed that to the optimized microstructure, in particular to the columnar growth of the electrolyte film.

2. Discussion

The results briefly described in the above chapter include both barium cerate, barium zirconate and barium cerate-zirconate perovskite films. Moreover, the content of the acceptor-type dopant in the analysed perovskites is between 0 and 0.2. The supports on which the films were deposited were of different types: insulating, semiconducting or metallic, as well as of different morphologies: amorphous, polycrystalline and single-crystalline. The films differed in thickness (between nanometers and a few micrometres), microstructure, density, etc. Some films were annealed after the deposition whereas the others were not. All these make the comparison of their properties very difficult if possible. Nevertheless, in the course of the discussion, we will attempt to find some common features of these films. In particular, we intend to trace indications of a possible influence of the strain on the electrical properties of the films. It should be stressed that in the majority of cases reported in the above chapter, strain and/or stress have not been considered by the authors as an important factor. First of all, we will start by collecting (Table 1) the selected conditions of the films preparation and their electrical properties.

Electrical properties of acceptor-doped barium zirconate and/or barium cerate films in comparison with their bulk counterparts span all possible variations. The conductivity values are either higher, comparable or lower than that of ceramic samples. The same applies to the activation energy of conductivity. To study why thin films exhibit such a wide range of electrical properties one should first recognize the factors which may influence these properties. While the conductivity in particular conditions (temperature and atmosphere) of bulk ceramic materials depend on their chemical composition, crystal structure, defect chemistry and microstructure, in the case of thin films additional factors play an important role. They are, among others, the chemical composition and structure of the substrate which influences the nature of the substrate-film interface, substrate morphology, the strain present in the interface between the substrate and the film, strain related to the thermal coefficient mismatch, and thickness of the film. Generally speaking, the properties of films are determined by the presence of interfaces which may be strained. What makes the analysis even harder, all the factors mentioned above are not independent one from another.

Table 1. Selected conditions of the films preparation and their electrical properties. BZY20 signifies $\text{BaZr}_{0.8}\text{Y}_{0.2}\text{O}_{3-\delta}$, BZY15— $\text{BaZr}_{0.85}\text{Y}_{0.15}\text{O}_{3-\delta}$, BZY10— $\text{BaZr}_{0.9}\text{Y}_{0.1}\text{O}_{3-\delta}$, BCY20— $\text{BaCe}_{0.8}\text{Y}_{0.2}\text{O}_{3-\delta}$, BZC40— $\text{BaZr}_{0.6}\text{Ce}_{0.4}\text{O}_3$, BC— $\text{BaCeO}_{3-\delta}$, BCZY712— $\text{BaCe}_{0.7}\text{Zr}_{0.1}\text{Y}_{0.2}\text{O}_{3-\delta}$. PLD—pulsed laser deposition, EBD—electron beam deposition, ALD—atomic layer deposition, PAD—powder aerosol deposition.

| Deposition Method | Film | Substrate, Substrate Temperature and/or Annealing Temperature | Electrical Properties |
|-------------------|------------------------|--|--|
| PLD [24] | BZY20 | (110) NdGaO_3 , 700 °C | Conductivity in very thin films is higher and its activation energy is lower (0.50) than in thicker films (0.80 eV). The strain and space charge layer is important. |
| PLD [25] | BZY20 buffer: BZC40 | (100) MgO , 750 °C | Conductivity comparable to bulk samples, the activation energy (0.39–0.47 eV) depends on the strain. |
| PLD [28] | BZY20 | (100) MgO ($\bar{1}\bar{1}02$) Al_2O_3 600 °C | The conductivity of both films is higher than that of the bulk sample, the conductivity of the film on Al_2O_3 is lower than on MgO ; activation energy 0.63 eV. |
| PLD [29] | BZY20 | (100) MgO , amorphous SiO_2 780 °C | The conductivity of BZY20 on MgO is comparable, while that of BZY on silica is 2 orders of magnitude lower than that of the bulk; activation energy: (0.45 and 1.2 eV); nano-grain structure considered as the source of high resistance. |

Table 1. Cont.

| Deposition Method | Film | Substrate, Substrate Temperature and/or Annealing Temperature | Electrical Properties |
|------------------------------|----------------|---|---|
| PLD [33] | BZY15 | (100) MgO, 700 °C | Conductivity is up to 3 orders of magnitude lower than the microcrystalline bulk solid, activation energy 0.79 eV; nano grain structure considered as the source of high resistance. |
| PLD [30] | BZY20 | (100) MgO, 600 and 900 °C | The activation energy of conductivity in the film deposited at higher temperature (0.45 eV for 900 °C, 0.51–0.53 eV for 600 °C) is lower. |
| | | amorphous SiO ₂ , 400–900 °C | Lower conductivity and higher activation energy (1.12 eV) than that on MgO; the crystallinity and microstructure of the film strongly influenced the conductivity. |
| PLD [31] | BCY10 | (100) MgO, 600 °C | Below 700 °C proton conduction dominates, activation energy 0.92 eV. |
| PLD [32] | BZY15 | (100)MgO, (110)GdScO ₃ , (001)SrTiO ₃ , (110)NdGaO ₃ , (1102)Al ₂ O ₃ , (012) LaAlO ₃ 600–800 °C; for conductivity measurements, the films were annealed at 700 °C for 30 min | Conductivity comparable to bulk samples, but lower than the best films ([28]); activation energy in wet air 0.65 eV, 0.47 eV in wet 5% H ₂ /Ar; Defects and film stoichiometry are considered as important factors influencing the conductivity, a possible influence of strain related to TEC mismatch. |
| EBD [26] | BC | Steel, Invar, Inconel, Glass Sealing Alloy, 600 °C | The conductivity, perpendicular to the substrate in dry air is comparable but lower than that of the bulk ceramics. The activation energy is between 0.6 and 1.1 eV. |
| Magnetron sputtering [34,35] | BZY16 | polycrystalline Al ₂ O ₃ covered with Pt ₃ Ti current collector, 250 °C, annealing at 675 °C for 12 h | The conductivity perpendicular to the substrate in dry air is lower than that of the bulk ceramics. The activation energy of conductivity of the films and the bulk sample below 400 °C is 0.62 eV and 0.52 eV, respectively. |
| ALD [37] | BZY20 | amorphous SiO ₂ , RT, annealing at 700–900 °C for 10 h | The activation energy of the conductivity in ambient air was 0.80 eV. The structural distortions and grain separation increase the resistance of films. |
| ALD [38] | BZY20 | (100) Si, RT, annealing at 800 °C for 2 h | The activation energy of the conductivity in ambient air was 0.80 eV. |
| PAD [39,40] | BZY20 BCY20 | polycrystalline Al ₂ O ₃ with a platinum interdigital electrode, RT, | The conductivity of as-prepared films is low, while E _A is high (1.73 eV and 1 eV for BZY20 and BCY20, respectively. Annealing causes an increase in conductivity and a decrease in activation energy (0.88 eV and 0.54 eV). |
| Ink-jet [41] | BZY10 | (100) Si covered with platinum, Al ₂ O ₃ , annealing at 1000 °C | Dielectric permittivity ~36 The conductivity of the films on alumina is lower than that of the bulk ceramics, the activation energy below 400 °C is 0.56 eV, above this temperature: 1.46 eV. |
| Spray pyrolysis [42] | BCZY712 | polycrystalline Al ₂ O ₃ , 250 °C, annealing at 700–1000 °C | The activation energy of DC conductivity in wet air is 0.73 eV. |

2.1. Microstructure and Morphology

Given the results reported in the literature and gathered in this brief review, the microstructure and morphology of the films strongly influence their electrical properties. There are a few examples of epitaxial films with higher proton conductivity than that of dense polycrystalline bulk ceramics. The best epitaxial barium zirconate films were obtained using the PLD method. The most spectacular case is shown in the work of



Pergolesi et al. [28] in which the highest measured in-plane proton conductivity was observed in an epitaxial, approximately 1 μm thick, $\text{BaZr}_{0.8}\text{Y}_{0.2}\text{O}_{3-\delta}$ deposited on the insulating MgO single-crystalline substrate. The authors reported two orders of magnitude higher conductivity of this film compared to the bulk. On the other hand, the proton conductivity of the film deposited on the single crystalline Al_2O_3 was four times lower than that of BZY20 on MgO but still higher in comparison with the bulk ceramics. Although other authors studying epitaxial layers deposited by PLD showed lower film conductivity than those of Pergolesi et al., one may say that the conductivity of BZY deposited on single-crystalline MgO is higher than that of the films deposited on other supports, e.g., Al_2O_3 or strontium titanate [32]. On the whole, epitaxial films conduct much better than polycrystalline ones, which at first sight may be related to the presence of blocking grain boundaries typical of barium zirconate ceramic proton conductors. What is, however, intriguing is a wide range of conductivities reported by the authors in the films, namely, the conductivity in BZY20 at 400 $^\circ\text{C}$ was of the order of 10^{-2} [28], 10^{-3} [38], 10^{-4} [40] and 10^{-6} $\text{S}\cdot\text{cm}^{-1}$ (the latter value was found in BZY15) [33]. Even though the atmospheres in which particular measurements were performed were not identical, a difference of four orders of magnitude is much larger than the range of conductivity of bulk ceramics variations. What is more, in some cases, although the values of conductivity of differently prepared thin films differed, the activation energy of conductivity was the same. Such a case was observed by Pergolesi et al. in epitaxial BZY20 films deposited on MgO and Al_2O_3 . Because of the same activation energy (0.63 eV) of conductivity in the films differing in the crystal orientation and strain caused by the unit cell parameter mismatch, they postulated that these factors affect only the pre-exponential factor of conductivity, that is, mainly the charge carriers concentration. Other examples are two different ALD BZY20 films. Similar activation energies of conductivity (~ 0.80 eV) were observed in the non-epitaxial BZY20 films deposited with the ALD method on amorphous SiO_2 [37] and (100) Si [38]. In these cases, the thin films after the deposition process were annealed at temperatures between 700 and 900 $^\circ\text{C}$, however, the annealing did not influence strongly the activation energy. In contrast to these examples, several results show a rather strong relation between the activation energy of conductivity and the microstructural characteristics of the films. For example, Kim et al. [30] showed that increasing the substrate temperature from 600 to 900 $^\circ\text{C}$, which affected the degree of epitaxial crystallization of the film, changed also the activation energy of conductivity from 0.53 to 0.45 eV. Moreover, the same authors observed much higher activation energy (1.12 eV) in the polycrystalline, non-oriented film deposited on the amorphous silica substrate.

Summing up, the activation energy of the conductivity of various BZY20 films, determined in the temperature range below 400 $^\circ\text{C}$ in an atmosphere containing water vapour, is in the range between 0.39 and 1.2 eV, whereas the values of the conductivity at 400 $^\circ\text{C}$ may differ by four orders of magnitude. It should be emphasized that the values of conductivity and activation energy of conductivity differ also in seemingly similar epitaxial BZY films deposited with the same method on the same substrates. Though the difference between the number and structure of highly resistive grain boundaries among the films is an important factor influencing their conductivity, a wide variety of electrical properties indicates that also other aspects may be equally relevant.

2.2. Film Thickness

In the case of epitaxial or strongly oriented thin films of thickness below 1 μm , deposited using the PLD method, the influence of the film thickness on the conductivity was emphasized by Shim et al. [29] and Yang et al. [24]. On the other hand, Pergolesi et al. [28] did not observe a dependence of the conductivity on the thickness of the film, however, they studied films of the thickness between 0.5 and 1.5 μm . Shim et al. found that the conductivity of the films deposited on MgO decreased with increasing film thickness. The dependence was strong for the thinnest films, however, an influence of the thickness on the activation energy (~ 0.45 eV) of conductivity was not observed. The thinnest, 60 nm



and 110 nm thick films were epitaxial, oriented with (100) plane parallel to the substrate surface, whereas the thicker ones were polycrystalline. The authors explained a decrease in conductivity with increasing film thickness with the formation of nanograins in the thicker films. Yang et al. studied BZY20 films deposited on (110) NdGaO₃. The films, regardless of their thickness which was between 5 and 500 nm, were epitaxial and oriented in the same way as the films reported by Shim et al. The authors observed the highest conductivity in the 10 nm thick films, whereas a further increase of the thickness resulted in decreasing conductivity. In contrast to the observations of Shim et al., they found that the conductivity of the very thin films (10–20 nm) was characterized by lower activation energy (0.50–0.55 eV) in comparison with the 100–500 nm films (0.75–0.80 eV). Yang et al. postulated that the presence of two interface layers influences strongly the conductivity of the film. One interface layer is highly conducting and forms between the substrate and the film. The high conductivity of this layer is related to the strain and interfacial defects which enable a higher concentration of charge carriers, i.e., proton defects. Another interface layer is a negative space-charge layer at the interface with the electrodes. This is connected with the presence of a transverse electric field directed from the thin film surface and causes the lowering of the charge carrier concentration. While the works of Shim et al. and Yang et al. show qualitatively similar results, they offer different explanations of the observed thickness dependence of conductivity. Moreover, one should also have in mind the fact that the highest conductivity ever observed in a BZY film was found in that of quite a large thickness (1 μm) [28], whereas in many cases, thinner, only a few tens of nanometers thick, films conducted much worse.

Summing up, the observed dependence of film conductivity on their thickness shows that not only do the typical barium zirconate grain boundaries determine the film properties but also the properties of the interfaces are essential. They include film/support-, film/buffer layer/support interface, film/electrode interface and film/atmosphere interface. It should be stressed that these interfaces usually are strained and the strain may depend on temperature and atmosphere.

2.3. Interfaces

The importance of the interfaces between different materials cannot be overestimated since the discovery of the n-p semiconductor junction. Nevertheless, ceramic proton conductors are quite complex materials, so that the knowledge of their interactions with other materials is limited. Recently, it has been reviewed in the work by Chiara et al. [44]. The junction between barium zirconate and another material may be viewed as consisting of the interface itself and the space charge layer. The former is ~0.2 nm thick, while the latter may extend for 1–2 nm in barium zirconate [45]. Saeed et al. [46] using ab-initio methods found that nanostructured SrTiO₃/BaZrO₃ interfaces can be enriched in proton defects which, in turn, leads to higher proton conductivity in comparison to individual phases. Simultaneously, the space charge region is depleted in proton defects in comparison to the bulk region. Moreover, close to the interface between the materials, SrTiO₃ is tensely-while BaZrO₃ is compressively strained, which influences the segregation of defects (v_{O}^{\bullet} , $\text{OH}_{\text{O}}^{\bullet}$) and the size of the space charge region. What should be also stressed, the authors found that contrary to grain boundaries, the equilibration of dopants in these heterointerfaces is much less important in comparison with grain boundaries. The presence of the interface layer enriched in proton defects in nanostructured SrTiO₃/BaZrO₃ interfaces was proposed to be a possible source of enhancing the proton conductivity of the system. On the other hand, Polfus et al. [45] studied the MgO and yttrium-doped barium zirconate interfaces. They showed that similarly to SrTiO₃/BaZrO₃, in the MgO/BaZr_{0.9}Y_{0.1}O_{3-δ} interfaces proton defects accumulation occurs whereas the space charge layer is depleted in protons. In the BaZr_{0.9}Y_{0.1}O_{3-δ} films, the space charge layer width and potential strongly depend on whether the equilibration of the Y'_{Zr} defects is possible, or not. This indicates that the properties of thin films deposited on MgO should depend on the thermal history of the sample. For instance, the temperature of the substrate maintained during the

deposition process, cooling rate and post-deposition annealing may be crucial factors determining the thin film conductivity. This partially explains a wide distribution in the experimentally found properties of the BZY films deposited on the MgO substrates. In the case of the MgO/BaZr_{0.9}Y_{0.1}O_{3-δ} interfaces, although they are enriched in proton defects the activation energy for proton conductivity along the interface layer was found to be relatively high (~1 eV), so that, the proton conductivity in the interface cannot be expected to be high. Indeed, Fluri et al. [25] suggested that the interface layer a few nanometers thick does not contribute to the film conduction. The determination of the role of the interface between particular substrate materials and barium zirconate thin film requires further studies. For instance, in the case of the MgO/BZY interface, though the proton conduction appears to be low, the authors of [45] suggested that the presence of a quite high space charge layer potential may, in reducing conditions, cause an accumulation of electronic charge in the interface which may contribute to the total conductivity. This idea may be supported by the results of Pergolesi et al. [28] who observed the highest conductivity with the lowest activation energy in the thin films under the humidified 5% H₂ in Ar atmosphere, however, they excluded the possibility of a 2D conductivity contribution. On the other hand, Magrasó et al. [32] observed that the conductivity of BZY on MgO decreased with decreasing oxygen partial pressure and was the lowest in the atmosphere of humidified 5% H₂ 95% Ar. Nevertheless, the presence of an electric field in the space charge and/or interface region inevitably influences the transport properties. The interface between barium zirconate and NGO substrate was studied by Yang et al. [24] using electrochemical scanning microscopy. They observed different behaviour of the thin films 20 nm thick in comparison to these of 300 nm. In particular, thinner films were characterized by higher electrochemical activity and lower activation energy of conductivity. They interpreted them as related to the higher mobility of proton defects in the thinner films. As proposed by the authors, the higher mobility may be caused by the presence of an array of misfit dislocations formed as a result of structural strain at the substrate–film interface, which provides new proton transport paths in which proton trapping is less significant.

Another type of interface present in the case of thin films are, as was suggested by Yang et al. [24], interfaces between the thin film and the metallic electrode. If the junction between a metal and an oxide is a Schottky junction, it is accompanied by the space charge region formation, which inevitably influences the thin film conducting properties. Saed and Bjørheim [47] studied the role of space charge at metal/metal oxide interfaces relevant for proton ceramic fuel cells. In particular, they studied the interfaces between BaZrO₃ and various metals, e.g., Ni, Ni, Pd, Pt, Cu, Ag, and Au. The electrostatic potential difference between the interface and bulk BaZrO₃ depends on the metal work function and on temperature. In the case of platinum, which is usually used as an electrode material the potential difference is negative and decreases, i.e., becomes more negative, with increasing temperature. A negative potential result in the enrichment in oxygen vacancies is accompanied by a decrease in the concentration of proton defects in the region close to the interface. In the case of metals with lower work function, e.g., Ag, Cu and Ni, the space-charge region is depleted in positive charge carriers, that is, both in oxygen vacancies and proton defects. Therefore, regardless of which metal forms a junction with barium zirconate, the proton conductivity of the layer being in contact with metal is expected to diminish. Another aspect of barium zirconate-metal interfaces is the chemical reactivity. Nanostructures based on metals supported on oxides or oxides supported on metals are used in various fields for their catalytic activity. Recently, Jennings et al. [48] observed that the presence of nickel promotes thin barium zirconate film decomposition, whereas Fe prevents decomposition.

2.4. Strain

Another factor related to the presence of substrate/barium zirconate interfaces is strain. The discussion on the strain influence on the properties of proton conductors is not straightforward because only a few partially contradicting reports concerning this

field have been published so far. In the case of bulk materials, Ottochian et al. [49], using molecular dynamics showed that compressive isotropic pressure favours proton diffusion by diminishing the oxygen–oxygen distance without affecting the crystal symmetry. On the other hand, with a biaxial strain, a similar effect was observed only in the case of a moderate compressive strain, while for high strain, because of symmetry reduction a strong localization of protons away from the Zr/Y cations was observed. This work was in contradiction with the earlier experimental work reported by Chen et al. [50] who found that the bulk proton conductivity of $\text{BaZr}_{0.9}\text{Y}_{0.1}\text{O}_{2.95}$ decreased under a compressive pressure. The authors also correlated the activation energy of proton conduction with strain, that is, the E_a decreased with the increase in lattice constant. This observation is in agreement with the work published by Fluri et al. [25] concerning the strained films of BZY20 deposited on MgO, however, these results showed that the influence of strain on proton conduction is more complex. Although the tensile strain which increases the distance between oxygen ions makes the proton migration more difficult, however, if the vicinity of the YO_6 octahedra is concerned, this type of strain lowers the proton trapping energy. The authors concluded that there exists an optimal tensile strain in which the proton conductivity attains a maximum.

Apart from a direct influence on the proton migration barriers, other effects which may be related to the strain have been proposed. As was mentioned above, they include the strain-induced dislocation formation and the influence of strain on the energy of defect formation, thus on the segregation of defects and the size of the space charge region. In the hetero-epitaxial thin films in which a small lattice mismatch is present, the lattice of the thin film is strained, while for the higher lattice mismatch, the strain causes the formation of dislocations during the thin film growth. In both cases, the thin film close to the interface with the substrate is strained, since the dislocation itself generates the strain field around the dislocation line. This is an important effect because the elastic energy of a dislocation is distributed in the region of a few nanometers around the core. Moreover, the misfit dislocations form an array of dislocations that may be distant one from another for 10–20 nm. The influence of dislocations and the strain related to them on defect chemistry was described in a few oxide systems. For example, the studies on dislocations in the $\text{La}_{0.7}\text{Sr}_{0.3}\text{MnO}_3$ films on the LaAlO_3 substrate were reviewed by Sandiumenge [51]. The strain present in the dislocation core and around, in the case of oxides, influences the energy of oxygen vacancy formation. Similarly, the energy of formation of other charged defects, e.g., proton defects is modified through their interaction with the electrostatic field related to strain/stress. In strontium titanate, the formation energy of oxygen vacancies in the dislocation core was found to be much lower than that in the bulk crystal [52]. In the case of barium zirconate, the influence of dislocations has not been reported yet, however it is known that the compressive strain promotes the formation of oxygen vacancies whereas increases the formation energy of proton defects [46]. The influence of strain on the defect energy formation changes the concentration of defects in strained regions, therefore it affects the conductivity corresponding to charged defect transport. The strain influence on defect formation energy, that is, on defect concentration may be supported by the results of Pergolesi et al. who found that the strain caused by the unit cell parameter mismatch affects only the pre-exponential factor of conductivity [28]. Moreover, Yang et al. suggested that a high concentration of proton defects in interface layers form owing to the presence of strain and interfacial defects [24]. What is important, such a type of influence of strain on the charge carrier concentration affects equally the conductivity, regardless of the direction. This means that it is the same in the case of the current oriented in-plane and out-of-plane. Exner et al. [39] studied the polycrystalline, relatively thick films of yttrium-doped barium zirconate and cerate deposited using the powder aerosol deposition method. This deposition process results in the formation of strongly compressively strained grains. The authors observed a very high increase of conductivity caused by annealing at high temperatures. They interpreted it as owing to the strain release occurring at high temperatures. It may be connected with an increased proton defect formation energy in

the compressed lattice, however, at high temperatures also other processes influencing the conductivity occur, that is grain and grain boundary changes. Apart from the influence of dislocations on the defect formation energies, the presence of an array of dislocations may also influence the mobility of charge carriers. It was suggested in [24] that misfit dislocation formation may provide the proton transport paths without proton trapping. So-called pipe-diffusion along the dislocation lines is known in metals and was also observed in other systems [53]. The knowledge on dislocations and pipe-diffusion in oxides is limited. Since an oxide is composed of at least two different ions, the pipe-diffusion can lead to further chemical phenomena like extended defect nucleation, as it was found in the case of Y_2O_3 [54]. On the other hand, Marrocchelli et al. [2], showed that though the dislocation lines in strontium titanate are enriched in oxygen vacancies, the mobility of ions is low and the pipe-diffusion along the dislocation line is expected to be slow.

Finally, if the strain in the thin films deposited on different substrates is concerned, one should also take into account the additional strain which originates from the thermal coefficients (TEC) difference. For example, the structural misfit between the MgO and BaZrO₃ introduces a slightly compressive in-plane strain, while the TEC difference is related to additional compression or tension below or above the temperature of film deposition. Taking into account this temperature-dependent contribution to the total strain makes the whole picture even more complex.

3. Conclusions

The results reviewed and discussed above illustrate the complexity of the phenomena and conditions which may determine the properties of thin films. First of all, the microstructure and morphology of the thin films determine their electrical properties. Secondly, the presence of interfaces between barium zirconate/cerate and the substrate and metallic electrodes, space-charge layers as well as the strain induced by a structural difference between substrate and film materials, misfit dislocations and the temperature affect the conductivity of the film.

The microstructure and morphology of the films, similarly to the bulk ceramic BZY strongly affect the conductivity because of the high resistivity of grain boundaries. Epitaxial BZY thin films have higher conductivity in comparison to the polycrystalline ones, however, the differences between particular epitaxial films are also high.

In the interfaces, space charge regions and strained regions, both the charge carrier's concentration and their mobility change. The charge carrier concentration is affected through the influence on the energy of oxygen vacancies, proton- or other mobile defect formation. The mobility of charge carriers is influenced by the distance between particular atoms, therefore it depends on the type of strain and the orientation of the strain and the current.

Given the strong influence of film microstructure on the electrical properties, the contribution of the interface layers, space-charge layers, and strain-modified layers to the total conductivity in some cases may not be clearly observed.

Author Contributions: Conceptualization, M.G., G.L.; formal analysis, M.G., K.B., M.S., M.S.C.C., G.L.; investigation, M.G., P.W., T.M., W.S., D.J., M.S.C.C., G.L.; writing—original draft preparation, M.G., P.W., M.S.C.C.; writing—review and editing, M.G., P.W., T.M., W.S., D.J., M.S.C.C., G.L., K.B., M.S., supervision, M.G., G.L.; project administration, M.G., K.B., G.L.; funding acquisition, M.G., G.L. All authors have read and agreed to the published version of the manuscript.

Funding: The research was financially supported by Research Council of Lithuania (LMTLT), agreement No. S-LL-18-3 and the National Science Centre, Poland project No. 2017/27/L/ST5/03185.

Conflicts of Interest: The authors declare no conflict of interest.

References

1. Greene, J.E. Tracing the 5000-year recorded history of inorganic thin films from ~3000 BC to the early 1900s AD. *Appl. Phys. Rev.* **2014**, *1*, 41302. [[CrossRef](#)]
2. Grove, W.R. VII. On the electro-chemical polarity of gases. *Philos. Trans. R. Soc. Lond.* **1852**, *142*, 87–101. [[CrossRef](#)]
3. Eckertová, L. Introduction. In *Physics of Thin Films*; Springer: New York, NY, USA, 1977; pp. 9–10.
4. Hoffman, R.L.; Norris, B.J.; Wager, J.F. ZnO-based transparent thin-film transistors. *Appl. Phys. Lett.* **2003**, *82*, 733–735. [[CrossRef](#)]
5. Trolier-Mckinstry, S.; Muralt, P. Thin film piezoelectrics for MEMS. *J. Electroceram.* **2004**, *12*, 7–17. [[CrossRef](#)]
6. Venkatasubramanian, R.; Siivola, E.; Colpitts, T.; O'Quinn, B. Thin-film thermoelectric devices with high room-temperature figures of merit. *Nature* **2001**, *413*, 597–602. [[CrossRef](#)]
7. Aberle, A.G. Thin-film solar cells. *Thin Solid Film.* **2009**, *517*, 4706–4710. [[CrossRef](#)]
8. Wang, J.; Neaton, J.B.; Zheng, H.; Nagarajan, V.; Ogale, S.B.; Liu, B.; Viehland, D.; Vaithyanathan, V.; Schlom, D.G.; Waghmare, U.V.; et al. Epitaxial BiFeO₃ multiferroic thin film heterostructures. *Science* **2003**, *299*, 1719–1722. [[CrossRef](#)]
9. Shockley, W.; Bardeen, J. Energy bands and mobilities in monatomic semiconductors. *Phys. Rev.* **1950**, *77*, 407–408. [[CrossRef](#)]
10. Smith, C.S. Piezoresistance effect in germanium and silicon. *Phys. Rev.* **1954**, *94*, 42–49. [[CrossRef](#)]
11. Welsch, J.; Hoyt, J.L.; Takagi, S.; Gibbons, J.F. Strain dependence of the performance enhancement in strained-Si n-MOSFETs. In *Technical Digest, Proceedings of the IEEE International Electron Devices Meeting, San Francisco, CA, USA, 11–14 December 1994*; IEEE: Piscataway, NJ, USA, 1994; pp. 373–376. [[CrossRef](#)]
12. Bedell, S.W.; Khakifirooz, A.; Sadana, D.K. Strain scaling for CMOS. *MRS Bull.* **2014**, *39*, 131–137. [[CrossRef](#)]
13. Sun, Y.; Thompson, S.E.; Nishida, T. Physics of strain effects in semiconductors and metal-oxide-semiconductor field-effect transistors. *J. Appl. Phys.* **2007**, *101*, 104503. [[CrossRef](#)]
14. Schlom, D.G.; Chen, L.Q.; Fennie, C.J.; Gopalan, V.; Muller, D.A.; Pan, X.; Ramesh, R.; Uecker, R. Elastic strain engineering of ferroic oxides. *MRS Bull.* **2014**, *39*, 118–130. [[CrossRef](#)]
15. Li, J.; Shan, Z.; Ma, E. Elastic strain engineering for unprecedented materials properties. *MRS Bull.* **2014**, *39*, 108–114. [[CrossRef](#)]
16. Bhatt, M.D.; Lee, J.S. Effect of lattice strain on nanomaterials in energy applications: A perspective on experiment and theory. *Int. J. Hydrog. Energy* **2017**, *42*, 16064–16107. [[CrossRef](#)]
17. Tuller, H.L.; Bishop, S.R. Point defects in oxides: Tailoring materials through defect engineering. *Annu. Rev. Mater. Res.* **2011**, *41*, 369–398. [[CrossRef](#)]
18. Santiso, J.; Burriel, M. Deposition and characterisation of epitaxial oxide thin films for SOFCs. *J. Solid State Electrochem.* **2011**, *15*, 985–1006. [[CrossRef](#)]
19. Shi, Y.; Bork, A.H.; Schweiger, S.; Rupp, J.L.M. The effect of mechanical twisting on oxygen ionic transport in solid-state energy conversion membranes. *Nat. Mater.* **2015**, *14*, 721–727. [[CrossRef](#)] [[PubMed](#)]
20. Kushima, A.; Yildiz, B. Oxygen ion diffusivity in strained yttria stabilized zirconia: Where is the fastest strain? *J. Mater. Chem.* **2010**, *20*, 4809–4819. [[CrossRef](#)]
21. Aguesse, F.; Axelsson, A.K.; Reinhard, P.; Tileli, V.; Rupp, J.L.M.; Alford, N.M.N. High-temperature conductivity evaluation of Nb doped SrTiO₃ thin films: Influence of strain and growth mechanism. *Thin Solid Film.* **2013**, *539*, 384–390. [[CrossRef](#)]
22. Kreuer, K.D. Aspects of the formation and mobility of protonic charge carriers and the stability of perovskite-type oxides. *Solid State Ion.* **1999**, *125*, 285–302. [[CrossRef](#)]
23. Kreuer, K.D. On the complexity of proton conduction phenomena. *Solid State Ion.* **2000**, *136–137*, 149–160. [[CrossRef](#)]
24. Yang, N.; Cantoni, C.; Foglietti, V.; Tebano, A.; Belianinov, A.; Strelcov, E.; Jesse, S.; Di Castro, D.; Di Bartolomeo, E.; Licoccia, S.; et al. Defective interfaces in yttrium-doped barium zirconate films and consequences on proton conduction. *Nano Lett.* **2015**, *15*, 2343–2349. [[CrossRef](#)]
25. Fluri, A.; Marcolongo, A.; Roddatis, V.; Wokaun, A.; Pergolesi, D.; Marzari, N.; Lippert, T. Enhanced proton conductivity in Y-doped BaZrO₃ via strain engineering. *Adv. Sci.* **2017**, *4*, 1700467. [[CrossRef](#)] [[PubMed](#)]
26. Covarrubias, M.S.C.; Sriubas, M.; Bockute, K.; Winiarz, P.; Miruszewski, T.; Skubida, W.; Jaworski, D.; Bartmański, M.; Szkodo, M.; Gazda, M.; et al. Properties of barium cerate thin films formed using E-beam deposition. *Crystals* **2020**, *10*, 1152. [[CrossRef](#)]
27. Løken, A.; Ricote, S.; Wachowski, S. Thermal and chemical expansion in proton ceramic electrolytes and compatible electrodes. *Crystals* **2018**, *8*, 365. [[CrossRef](#)]
28. Pergolesi, D.; Fabbri, E.; D'Epifanio, A.; Di Bartolomeo, E.; Tebano, A.; Sanna, S.; Licoccia, S.; Balestrino, G.; Traversa, E. High proton conduction in grain-boundary-free yttrium-doped barium zirconate films grown by pulsed laser deposition. *Nat. Mater.* **2010**, *9*, 846–852. [[CrossRef](#)]
29. Shim, J.H.; Gür, T.M.; Prinz, F.B. Proton conduction in thin film yttrium-doped barium zirconate. *Appl. Phys. Lett.* **2008**, *92*, 2–5. [[CrossRef](#)]
30. Kim, Y.B.; Gür, T.M.; Jung, H.-J.; Kang, S.; Sinclair, R.; Prinz, F.B. Effect of crystallinity on proton conductivity in yttrium-doped barium zirconate thin films. *Solid State Ion.* **2011**, *198*, 39–46. [[CrossRef](#)]
31. Hosono, H.; Higuchi, T.; Hattori, T. Electrical and structural properties of BaCe_{0.90}Y_{0.10}O_{3-δ} thin film on MgO (100) substrate. *J. Appl. Phys.* **2008**, *104*, 113704. [[CrossRef](#)]
32. Magrasó, A.; Ballesteros, B.; Rodríguez-Lamas, R.; Sunding, M.F.; Santiso, J. Optimisation of growth parameters to obtain epitaxial Y-doped BaZrO₃ proton conducting thin films. *Solid State Ion.* **2018**, *314*, 9–16. [[CrossRef](#)]

33. Bae, K.; Jang, D.Y.; Choi, H.J.; Kim, D.; Hong, J.; Kim, B.K.; Lee, J.H.; Son, J.W.; Shim, J.H. Demonstrating the potential of yttrium-doped barium zirconate electrolyte for high-performance fuel cells. *Nat. Commun.* **2017**, *8*, 1–9. [[CrossRef](#)]
34. Arab Pour Yazdi, M.; Briois, P.; Georges, S.; Costa, R.; Billard, A. Characterization of PCFC-electrolytes deposited by reactive magnetron sputtering; comparison with ceramic bulk samples. *Fuel Cells* **2013**, *13*, 549–555. [[CrossRef](#)]
35. Arab Pour Yazdi, M.; Briois, P.; Georges, S.; Shaula, A.L.; Cavaleiro, A.; Billard, A. Comparison of structural and electrical properties of barium zirconate pellets and thin films. *J. Electrochem. Soc.* **2010**, *157*, B1582. [[CrossRef](#)]
36. Wu, L.J.; Wu, J.M. Reduced leakage current and conduction mechanisms of sputtered platinum-doped lead barium zirconate thin films. *J. Phys. D Appl. Phys.* **2007**, *40*, 4948–4952. [[CrossRef](#)]
37. Park, J.S.; Kim, Y.B.; An, J.; Shim, J.H.; Gür, T.M.; Prinz, F.B. Effect of cation non-stoichiometry and crystallinity on the ionic conductivity of atomic layer deposited Y:BaZrO₃ films. *Thin Solid Film.* **2013**, *539*, 166–169. [[CrossRef](#)]
38. An, J.; Beom Kim, Y.; Sun Park, J.; Hyung Shim, J.; Gür, T.M.; Prinz, F.B. Fluorine contamination in yttrium-doped barium zirconate film deposited by atomic layer deposition. *J. Vac. Sci. Technol. A Vac. Surf. Film.* **2012**, *30*, 01A161. [[CrossRef](#)]
39. Exner, J.; Nazarenus, T.; Kita, J.; Moos, R. Dense Y-doped ion conducting perovskite films of BaZrO₃, BaSnO₃, and BaCeO₃ for SOFC applications produced by powder aerosol deposition at room temperature. *Int. J. Hydrogen Energy* **2020**, *45*, 10000–10016. [[CrossRef](#)]
40. Exner, J.; Nazarenus, T.; Hanft, D.; Kita, J.; Moos, R. What happens during thermal post-treatment of powder aerosol deposited functional ceramic films? Explanations based on an experiment-enhanced literature survey. *Adv. Mater.* **2020**, *32*, 1908104. [[CrossRef](#)]
41. Schneller, T.; Griesche, D. Inkjet printed Y-substituted barium zirconate layers as electrolyte membrane for thin film electrochemical devices. *Membranes* **2019**, *9*, 131. [[CrossRef](#)]
42. Dubal, S.U.; Jamale, A.P.; Bhosale, C.H.; Jadhav, L.D. Proton conducting BaCe_{0.7}Zr_{0.1}Y_{0.2}O_{2.9} thin films by spray deposition for solid oxide fuel cell. *Appl. Surf. Sci.* **2015**, *324*, 871–876. [[CrossRef](#)]
43. Yoo, Y.; Lim, N. Performance and stability of proton conducting solid oxide fuel cells based on yttrium-doped barium cerate-zirconate thin-film electrolyte. *J. Power Sources* **2013**, *229*, 48–57. [[CrossRef](#)]
44. Chiara, A.; Giannici, F.; Pipitone, C.; Longo, A.; Aliotta, C.; Gambino, M.; Martorana, A. Solid–solid interfaces in protonic ceramic devices: A critical review. *ACS Appl. Mater. Interfaces* **2020**, *12*, 55537–55553. [[CrossRef](#)]
45. Polfus, J.M.; Norby, T.; Bredesen, R. Proton segregation and space-charge at the BaZrO₃ (0 0 1)/MgO (0 0 1) heterointerface. *Solid State Ion.* **2016**, *297*, 77–81. [[CrossRef](#)]
46. Saeed, S.W.; Norby, T.; Bjørheim, T.S. Charge-carrier enrichment at BaZrO₃ /SrTiO₃ interfaces. *J. Phys. Chem. C* **2019**, *123*, 20808–20816. [[CrossRef](#)]
47. Saeed, S.W.; Bjørheim, T.S. The role of space charge at metal/oxide interfaces in proton ceramic electrochemical cells. *J. Phys. Chem. C* **2020**, *124*, 20827–20833. [[CrossRef](#)]
48. Jennings, D.; Ricote, S.; Caicedo, J.M.; Santiso, J.; Reimanis, I. The effect of Ni and Fe on the decomposition of yttrium doped barium zirconate thin films. *Scr. Mater.* **2021**, *201*, 113948. [[CrossRef](#)]
49. Ottochian, A.; Dezanneau, G.; Gilles, C.; Raiteri, P.; Knight, C.; Gale, J.D. Influence of isotropic and biaxial strain on proton conduction in Y-doped BaZrO₃: A reactive molecular dynamics study. *J. Mater. Chem. A* **2014**, *2*, 3127. [[CrossRef](#)]
50. Chen, Q.; Braun, A.; Ovalle, A.; Savaniu, C.-D.; Graule, T.; Bagdassarov, N. Hydrostatic pressure decreases the proton mobility in the hydrated BaZr_{0.9}Y_{0.1}O₃ proton conductor. *Appl. Phys. Lett.* **2010**, *97*, 041902. [[CrossRef](#)]
51. Sandiumenge, F. A multiscale perspective on misfit dislocations in oxide films. *Front. Mater.* **2019**, *6*, 13. [[CrossRef](#)]
52. Marrocchelli, D.; Sun, L.; Yildiz, B. Dislocations in SrTiO₃: Easy to reduce but not so fast for oxygen transport. *J. Am. Chem. Soc.* **2015**, *137*, 4735–4748. [[CrossRef](#)]
53. Garbrecht, M.; Saha, B.; Schroeder, J.L.; Hultman, L.; Sands, T.D. Dislocation-pipe diffusion in nitride superlattices observed in direct atomic resolution. *Sci. Rep.* **2017**, *7*, 46092. [[CrossRef](#)] [[PubMed](#)]
54. Gaboriaud, R.J. Dislocation core and pipe diffusion in Y₂O₃. *J. Phys. D Appl. Phys.* **2009**, *42*, 135410. [[CrossRef](#)]

